

Cite this: *RSC Adv.*, 2017, 7, 55835

Highly sensitive extended gate-AlGaIn/GaN high electron mobility transistor for bioassay applications

Xiangzhen Ding,^{ad} Bin Miao,^a Zhiqi Gu,^{ag} Baojun Wu,^e Yimin Hu,^e Hong Wang,^e Jian Zhang,^f Dongmin Wu,^{sa} Wenhui Lu^{sb} and Jiadong Li^{sc}

Herein, an extended gate-AlGaIn/GaN high electron mobility transistor (EG-AlGaIn/GaN HEMT) with a high sensitivity for bioassay has been developed. The major difference between the EG-AlGaIn/GaN HEMT transducer and a traditional AlGaIn/GaN HEMT transducer is the sensing region. By extending the gate electrode and separating the sensing region from the channel of the AlGaIn/GaN HEMT, our EG-AlGaIn/GaN HEMT has a much larger sensing area and therefore achieves a low limit of detection (0.1 pg mL^{-1}). Additionally, our transducer exhibits excellent linearity ($R^2 = 0.9934$) with a wide range (from 0.1 pg mL^{-1} to 100 ng mL^{-1}). We also demonstrate that the larger area of the extended sensing region can provide a larger current response of the transducer. The results give a proof-of-concept demonstration of the utilization of the EG-AlGaIn/GaN HEMT for trace-level biological detection.

Received 8th September 2017
Accepted 28th November 2017

DOI: 10.1039/c7ra10028k

rsc.li/rsc-advances

Introduction

Over the past few years, the field of biosensors based on ion-sensitive field effect transistors (ISFETs) has developed rapidly, which may assist humans in making point-of-care testing (PoCT) a reality.^{1,2} These ISFET based biosensors have exhibited marvellous properties, such as easier miniaturization, real-time and rapid responses, high sensitivity, compatibility with integrated circuit technology, and so on.^{1–3} On the other hand, the development of new materials broadens the diversity of the ISFET field. Recent studies of AlGaIn/GaN HEMTs have explored their possible application in bioassays,⁴ on account of their high electron sheet carrier concentration, biocompatibility, lack of ion diffusion, and so forth.⁵ Plenty of work has been done to detect various biological analytes, such as cells,⁶

deoxyribonucleic acid,⁷ antigens,^{8,9} virus inhibitors,¹⁰ mercury ions (Hg^{2+}),¹¹ 2,4,6-trinitrotoluene (TNT),¹² etc.

Just like with the ISFET based sensors, during the exploration of clinical applications, researchers found that there is a poor isolation between the device and the biological environment, which presents the issue of reliability, especially when the sensing surface is undergoing reiterative rinses.^{13–15} Moreover, the absence of electrical reproducibility and reliability limits the applications of FET based biosensors, as these are significant parameters with respect to sensors.^{13–15} To overcome these issues, the extended gate field effect transistor (EG FET) was proposed as a solution in 1983.¹⁶ This structure enables people to pursue a better electrical performance of the amplification component, independently of the tailored sensing component, and *vice versa*. Additionally, a much simpler encapsulation solution can be used to make the amplification component free from most of the undesirable interferences like light and temperature. Since then, this novel structure has proved quite useful for different fields like genetic analysis,¹⁷ immunoassay,¹⁸ urinalysis,¹⁹ and so on. However, to the best of our knowledge, this structure has not been demonstrated with AlGaIn/GaN HEMTs, and so whether the EG-AlGaIn/GaN HEMT will achieve a comparable level of electrical performance compared with the Au gate AlGaIn/GaN HEMT⁸ or the biomolecule gate AlGaIn/GaN HEMT⁹ needs to be studied.

In this work, we have investigated the feasibility of developing the EG-AlGaIn/GaN HEMT for the detection of prostate specific antigen (PSA), which is considered to be the best biomarker for prostate cancer.^{20,21} A schematic illustration and plan view photomicrograph are shown in Fig. 1. The core of the EG-AlGaIn/GaN HEMT is separated into two parts: the extended

^ai-Lab, Suzhou Institute of Nano-Tech and Nano-Bionics, Chinese Academy of Sciences, Suzhou 215125, People's Republic of China. E-mail: jdli2009@sinano.ac.cn; dmwu2008@sinano.ac.cn

^bDepartment of Applied Physics, College of Science, Huzhou University, Huzhou 313000, People's Republic of China. E-mail: whlv2016@189.cn

^cState Key Laboratory of Applied Optics, Changchun Institute of Optics Fine Mechanics and Physics, Chinese Academy of Sciences, Changchun 130033, People's Republic of China

^dUniversity of Chinese Academy of Sciences, College of Materials Sciences and Opto-Electronic Technology, Beijing 100049, People's Republic of China

^eDivision of Nano-devices and Materials, Suzhou Institute of Nano-Tech and Nano-Bionics, Chinese Academy of Sciences (CAS), Suzhou 215123, People's Republic of China

^fNANO-X, Suzhou Institute of Nano-Tech and Nano-Bionics, Chinese Academy of Sciences, Suzhou 215125, People's Republic of China

^gSchool of Nano Technology and Nano Bionics, University of Science and Technology of China, Hefei, 230026, People's Republic of China



sensing region and the AlGaIn/GaN HEMT. The area of the sensing region is as large as $700\ \mu\text{m} \times 700\ \mu\text{m}$, which will be shown to be quite useful for the signal amplification later.

Experimental

Sensor fabrication

To begin with, the nitride heterostructure used in this study consists of a $1.5\ \mu\text{m}$ thick GaN buffer layer, an $18\ \text{nm}$ thick AlGaIn barrier layer and a $1.5\ \text{nm}$ thick GaN cap layer, which were grown by metal organic chemical vapor deposition (MOCVD) on the sapphire substrate. The wafer was then pre-cleaned using piranha solution (H_2SO_4 and H_2O_2 with a volumetric ratio of 3 : 1) and dried with nitrogen to ensure that it is clean. Inductively coupled plasma (ICP) etching with Cl_2/BCl_3 was performed to form the mesa isolation. The mesa height is around $40\ \text{nm}$ to make sure that the etching surpasses the 2DEG layer. In order to remove the native oxide layer, the wafer was then dipped into 10% (by volume) hydrochloric acid for 60 seconds. Ohmic contacts were formed with the typical multilayer of Ti/Al/Ni/Au by e-beam evaporation and annealed by a rapid thermal processing system under a flow of ambient nitrogen at $880\ ^\circ\text{C}$ for 45 seconds. To achieve an easier connection to the printed circuit board, the Ti/Ni/Au combination multilayer was evaporated overlapping above the ohmic contact electrode. A sputtering process was implemented to fabricate the gold extended gate. The wafer was encapsulated with SU8 except for the sensing region and connecting regions.

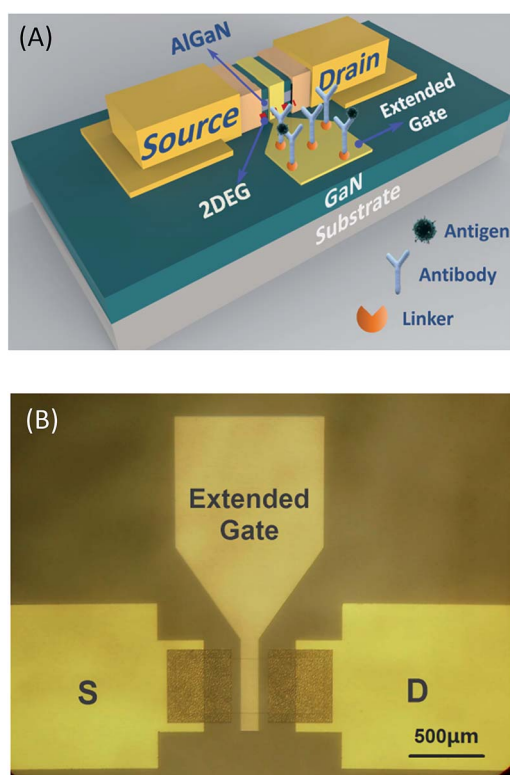


Fig. 1 The structure of the EG-AlGaIn/GaN HEMT: (A) a schematic illustration of the device, and (B) a plan view photomicrograph.

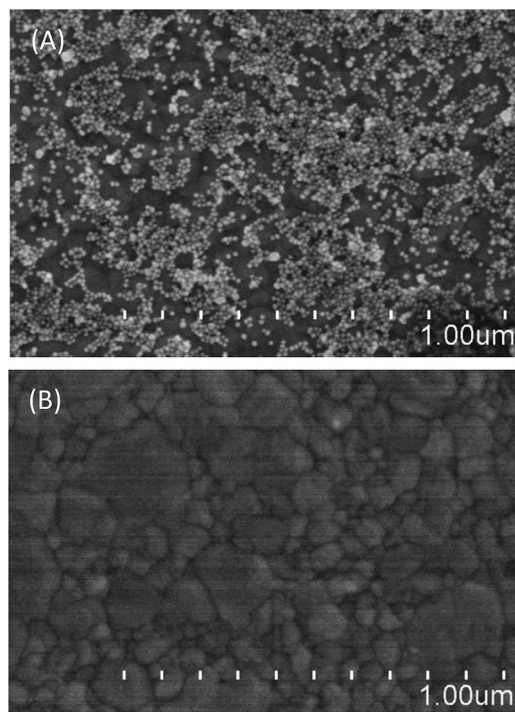


Fig. 2 Characterization of the device: (A) the adsorption of gold nanoparticles in the presence of successfully modified cysteamine, and (B) non-adsorption in the absence of cysteamine.

After dicing, the separate devices were mounted and electrically connected to the printed circuit boards.

Sensor modification

After the devices were fabricated and encapsulated, surface modification was implemented. The sensing region, namely the gold extended gate, was cleaned in an ozone/UV chamber for 30 minutes in the first instance. Shortly after cleaning, the gold extended gate was immersed in deoxygenated cysteamine aqueous solution for 6 hours at room temperature, to form ubiquitous thiol–gold bonds, and then rinsed with deionized

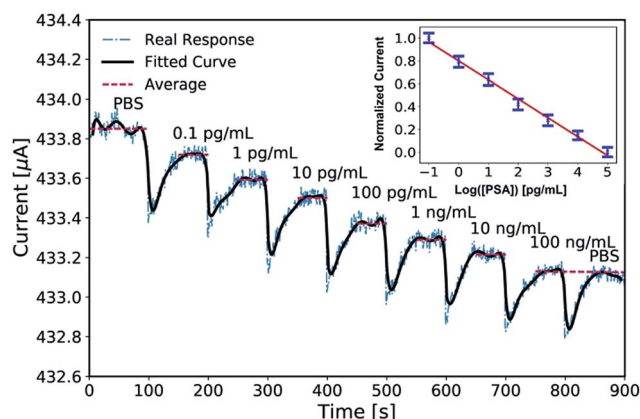
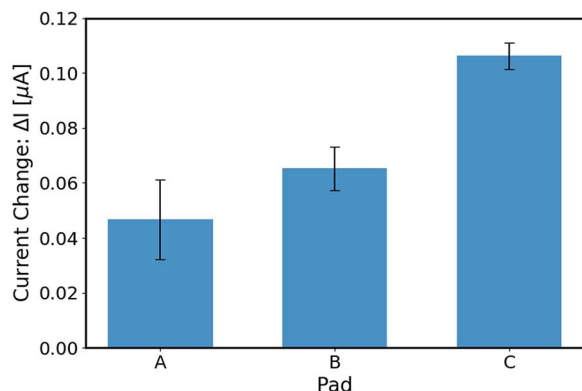


Fig. 3 The real-time detection of PSA (the red dashed lines are the average values and the bold black line is a fitted curve).



Table 1 Comparison of the electrical parameters of PSA biosensors based on AlGaIn/GaN HEMTs

The structure of the gate	Linear range	Limit of detection	Reference
Au gate	10 pg mL ⁻¹ to 10 ng mL ⁻¹	10 pg mL ⁻¹	Ref. 8
Biomolecule gate	0.1 pg mL ⁻¹ to 1 ng mL ⁻¹	0.1 pg mL ⁻¹	Ref. 11
Extended gate	0.1 pg mL ⁻¹ to 100 ng mL ⁻¹	0.1 pg mL ⁻¹	This work

**Fig. 4** The results of the current changes of three transducers with different sensing areas of the extended pads. The transducers were modified and measured with exactly the same conditions, and the experiments were repeated 3 times. (A) 400 μm × 400 μm, (B) 500 μm × 500 μm, and (C) 700 μm × 700 μm.

water. Glutaraldehyde solution with a concentration of 1.25% (by volume) was added into the lab-made reservoir for 2 hours to form a Schiff base between the aldehyde group and the amino group. Subsequently the device was rinsed with deionized water before the immobilization of 10 μg mL⁻¹ PSA monoclonal antibody. The device was finally incubated at 4 °C for 24 hours, ready for the following measurements. The cysteamine and glutaraldehyde were purchased from Sigma-Aldrich Co. LLC. (Shanghai, China). The gold nanoparticle solution was purchased from Nanjing XFNANO Materials Tech Co., Ltd (Nanjing, China). All of the measurements were performed in phosphate-buffered saline solution (PBS).

Results and discussion

Characterization

It has been well elucidated and demonstrated that there is a stable bond between amines and the surface of gold nanoparticles (Au NPs). This may stem from both the electrostatic adsorption between protonated amine groups and AuCl⁴⁻/AuCl²⁻, and a related complex of the form [AuCl(NH₂R)].²² Hence, Au NPs can be utilized to demonstrate the presence of cysteamine. Fig. 2 shows images resulting from scanning electron microscopy (SEM). The Au NPs were uniformly distributed upon the surface of the gold platform after being rinsed over five times and sonicated, as shown in Fig. 2A, whilst adsorbed Au NPs are hardly observed with the absence of cysteamine, as shown in Fig. 2B. The corresponding diameter of the gold nanoparticles is around 20 nm.

PSA detection

The device was finally connected to a Keithley 2636A instrument with a constant bias of 100 mV for the data acquisition. As shown in Fig. 3, the current response was quite steady in the first hundred seconds with the addition of 18 μL PBS, which indicates the stability of the device. Then, the current showed an instant abrupt decrease and then recovery to a steady level. This was due to the mechanical disturbance right after each step of titration by hand. For each cycle, within 60 seconds, the current achieved another steady level after completion of the antibody-antigen reaction. The obvious drop between every two titrations is around 100 nA. The red dashed lines in Fig. 3 depict the calculated average current during the steady stage, and the bold black line gives the fitted result of the real-time detection. At the end of the detection, a drop of PBS was titrated to verify the specificity of the device. The current response quickly returned to its previous level (*i.e.* at a PSA concentration of 100 ng mL⁻¹). The device also shows good linearity with an R^2 of 0.9934 in the inset, and the corresponding relationship is:

$$\Delta I/\Delta I_{\max} = -0.1658 \times \log([\text{PSA}]) + 0.7995 \quad (1)$$

where ΔI and ΔI_{\max} represent the current change due to a certain concentration of PSA ([PSA]), and the maximum current change during the whole test, respectively. Table 1 summarizes the PSA biosensors based on AlGaIn/GaN HEMTs. Compared to those of previous reports and our former work, the EG-AlGaIn/GaN HEMT showed a relatively wider linear range and retained a low limit of detection.

Discussion of the sensing area

It was reported that the presence of a gold layer may degrade the performances of AlGaIn/GaN HEMT transducers,²³ however based on the above results, it appears to be less influential than we expected for the EG-AlGaIn/GaN HEMT. The main factor of the EG-AlGaIn/GaN HEMT which may enhance the device performance in this situation, we suppose, is the sensing area. This is because it was reported that more surface receptors lead to a better electrical parameter of sensitivity,^{24,25} and a larger sensing area has more receptors. In order to elucidate the relationship between the sensing area of the EG-AlGaIn/GaN HEMT and its electrical characteristics, three different areas of the sensing pads were designed and modified (400 μm × 400 μm, 500 μm × 500 μm and 700 μm × 700 μm). The rest of the parameters of the EG-AlGaIn/GaN HEMT are identical. With the exact same conditions of modification, target PSA with different concentrations in buffer solutions, including 0.1 pg mL⁻¹, 1 pg mL⁻¹, 10 pg mL⁻¹, 100 pg mL⁻¹, 1 ng mL⁻¹, 10 ng mL⁻¹, and



100 ng mL⁻¹, were detected. The current changes (ΔI) of those three different sensing areas of the EG-AlGaIn/GaN HEMT transducers for PSA detection were obtained. In order to minimize the influences caused by the modification, each group of experiments was repeated 3 times. As shown in Fig. 4, the statistical average results give a quite explicit conclusion, that a larger area of the extended gate leads to a larger current change in our transducer. Based on the above observation, we hypothesize that the larger area of the extended gate gives a larger total amount of surface charge which causes a larger change of the gate voltage due to the capacitance coupling. This explains why our EG-AlGaIn/GaN HEMT exhibits good performance with a gold layer.

Conclusions

In summary, we have developed a highly sensitive EG-AlGaIn/GaN HEMT with a low limit of detection (0.1 pg mL⁻¹). Furthermore, our transducer exhibits an outstanding electrical performance, including excellent linearity ($R^2 = 0.9934$) with a wide range from 0.1 pg mL⁻¹ to 100 ng mL⁻¹. The device also shows stability and specificity in the presence of PBS. We also prove that a larger sensing area of the extended pad leads to a better electrical performance. It should also be noted that the extended gate can be tailored to various platforms for the corresponding detection of analytes, as long as the gate electrode is conductive. It is reasonable to believe that the EG-AlGaIn/GaN HEMT will be a promising diagnostic tool for further PoCT applications.

Conflicts of interest

There are no conflicts to declare.

Acknowledgements

This work has been supported by the NSFC Project (No. 61573346 and 61104226), the Youth Innovation Promotion Association CAS (2014278) and the State Key Laboratory of Applied Optics.

Notes and references

- 1 P. Bergveld, *IEEE Trans. Bio-Med. Electron.*, 1970, **17**, 70–71.
- 2 C. S. Lee, S. K. Kim and M. Kim, *Sensors*, 2009, **9**, 7111–7131.
- 3 A. de Moraes and L. Kubota, *Chemosensors*, 2016, **4**, 20.
- 4 R. Kirste, N. Rohrbach, I. Bryan, Z. Bryan, R. Collazo and A. Ivanisevic, *Annu. Rev. Anal. Chem.*, 2015, **8**, 149–169.
- 5 Y. Wang, P. Casal, S. C. Lee and W. Lu, *Device Research Conference (DRC)*, 71st Annual, 2013.
- 6 G. Steinhoff, B. Baur, G. Wrobel, S. Ingebrandt, A. Offenhäusser, A. Dadgar, A. Krost, M. Stutzmann and M. Eickhoff, *Appl. Phys. Lett.*, 2005, **86**, 033901.
- 7 B. S. Kang, S. J. Pearton, J. J. Chen, F. Ren, J. W. Johnson, R. J. Therrien, P. Rajagopal, J. C. Roberts, E. L. Piner and K. J. Linthicum, *Appl. Phys. Lett.*, 2006, **89**, 122102.
- 8 B. S. Kang, H. T. Wang, T. P. Lele, Y. Tseng, F. Ren, S. J. Pearton, J. W. Johnson, P. Rajagopal, J. C. Roberts, E. L. Piner and K. J. Linthicum, *Appl. Phys. Lett.*, 2007, **91**, 112106.
- 9 J.-d. Li, J.-j. Cheng, B. Miao, X.-w. Wei, J. Xie, J.-c. Zhang, Z.-q. Zhang and D.-m. Wu, *J. Micromech. Microeng.*, 2014, **24**, 075023.
- 10 Y.-W. Kang, G.-Y. Lee, J.-I. Chyi, C.-P. Hsu, Y.-R. Hsu, C.-H. Hsu, Y.-F. Huang, Y.-C. Sun, C.-C. Chen, S. Chun Hung, F. Ren, J. Andrew Yeh and Y.-L. Wang, *Appl. Phys. Lett.*, 2013, **102**, 173704.
- 11 J. Cheng, J. Li, B. Miao, J. Wang, Z. Wu, D. Wu and R. Pei, *Appl. Phys. Lett.*, 2014, **105**, 083121.
- 12 Y. Guo, X. Wang, B. Miao, Y. Li, W. Yao, Y. Xie, J. Li, D. Wu and R. Pei, *RSC Adv.*, 2015, **5**, 98724–98729.
- 13 Y. Hanazato, M. Nakako, S. Shiono and M. Maeda, *IEEE Trans. Electron Devices*, 1989, **36**, 1303–1310.
- 14 A. S. Poghosian, *Sens. Actuators, B*, 1997, **44**, 361–364.
- 15 L. T. Yin, J. C. Chou, W. Y. Chung, T. P. Sun and S. K. Hsiung, *Sens. Actuators, B*, 2000, **71**, 106–111.
- 16 J. V. D. Spiegel, I. Lauks, P. Chan and D. Babic, *Sens. Actuators*, 1983, **4**, 291–298.
- 17 C. P. Chen, A. Ganguly, C. Y. Lu, T. Y. Chen, C. C. Kuo, R. S. Chen, W. H. Tu, W. B. Fischer, K. H. Chen and L. C. Chen, *Anal. Chem.*, 2011, **83**, 1938–1943.
- 18 M. Kamahori, Y. Ishige and M. Shimoda, *Biosens. Bioelectron.*, 2007, **22**, 3080–3085.
- 19 W. Guan, X. Duan and M. A. Reed, *Biosens. Bioelectron.*, 2014, **51**, 225–231.
- 20 D. A. Healy, C. J. Hayes, P. Leonard, L. McKenna and R. O'Kennedy, *Trends Biotechnol.*, 2007, **25**, 125–131.
- 21 M. A. Najeeb, Z. Ahmad, R. A. Shakoor, A. M. A. Mohamed and R. Kahraman, *Talanta*, 2017, **168**, 52–61.
- 22 A. Kumar, S. Mandal, P. R. Selvakannan, R. Pasricha, A. B. Mandale and M. Sastry, *Langmuir*, 2003, **19**, 6277–6282.
- 23 M. Wirde, U. Gelius and L. Nyholm, *Langmuir*, 1999, **15**, 6370–6378.
- 24 M. S. Makowski, I. Bryan, Z. Sitar, C. Arellano, J. Xie, R. Collazo and A. Ivanisevic, *Appl. Phys. Lett.*, 2013, **103**, 13701.
- 25 Y. Xin, B. Munge, V. Patel, G. Jensen, A. Bhirde, J. D. Gong, N. K. Sang, J. Gillespie, J. S. Gutkind and F. Papadimitrakopoulos, *J. Am. Chem. Soc.*, 2006, **128**, 11199–11205.

